Deformation mechanism of a metal-organic framework glass under indentation

A. Qiao, T. To, M. Stepniewska, H. Tao, Laurent Calvez, Xianghua Zhang, M.M. Smedskjaer, Y. Yue

Deformation mechanism of a metal-organic framework glass under indentation

Ang Qiao,[ab‡] Theany To,[a‡] Malwina Stepniewska,[a] Haizheng Tao,[b] Laurent Calvez,[c] Xianghua Zhang,[c] Morten M. Smedskjaer, *[a] and Yuanzheng Yue *[ab]

Revealing the deformation mechanism of brittle materials under sharp contact loading (indentation) is important for their applications since this knowledge is crucial for identifying the origin of flaw and scratch formation on their surfaces. As a newly emerged glass family, metal-organic framework (MOF) glasses have not been studied concerning the mechanism of their indentation-induced deformation. Here, we explore this mechanism for ZIF-62 glass (a typical MOF glass system). The fractions of densification and shear flow during indentation were determined by atomic force microscopy, while the elastic deformation was analyzed via nanoindentation. The results show that ZIF-62 glass deforms primarily through densification and elastic deformation under the sharp contact loading. Pile-ups around indents were not observed, indicating that no or limited shear flow occurs in the glass during indentation. This behavior could be attributed to three structural factors, namely, high free volume, easily densified glass structure, and limited translational mobility of structural units.

1. Introduction

Inorganic glasses, except some metallic glasses, are well known for their inherent brittleness and low fracture toughness, leading to easy breakage under tensile stresses.[1] The ability of these glasses to resist the formation of surface indents, cracks, and scratches is crucial as these defects are the strength-limiting factors.[2-3] As such, hardness is an important glass property, which measures the glass' ability to resist sharp penetration under indentation loading. During the indentation process, three main deformation modes determine the indentation response of the glass, i.e., elastic deformation, shear flow, and densification.[4] Elastic deformation is a reversible deformation that can fully recover upon unloading.[4] Shear flow is a shear-induced volume conservative displacement, usually resulting in pile-ups around the indent.[5] Densification is a non-volume conservative compression that increases the density around the indent.[5] A comprehensive understanding of the indentation deformation mechanism is critical for improving the hardness and crack initiation resistance of glasses. The indentation deformation mechanism of oxide glasses has been well studied,[4-8] whereas such study has not been performed on metal-organic frameworks (MOF) glasses, which is a new family of melt-quenched (MQ) glasses.[9] The majority of currently known MOF glasses are derived from zeolitic imidazolate frameworks (ZIFs). ZIFs feature a zeolite-like three-dimensional framework structure, consisting of the metal node-ligand tetrahedral network, which are constructed by coordination bonds.[10,11] ZIF glasses possess a disordered, but fully polymerized network, similar to that of silica glass composed by [SiO_4] tetrahedral units,[12-14] but the former ones feature a higher degree of short-range disorder.[12]

Since the discovery of the MQ ZIF glasses, some studies have been carried out concerning their mechanical properties.[14-16] Originally, due to the lack of suitable methods for preparing bulk bubble-free ZIF glasses, only nanoindentation studies were performed on ZIF glasses with the nano- or micron-size to measure their elastic modulus and nano-hardness.[15] Recently, new synthesis strategies have emerged (vacuum hot-pressing methods), enabling the preparation of large size (~10 mm) bubble-free ZIF glasses. This makes it possible to measure the macro-scale mechanical properties of ZIF glasses, as done in three recent studies. First, Li *et al.* studied the creep resistance, strain-rate sensitivity, and scratch properties of a series of MQ ZIF glasses.[15] Second, Stepniewska *et al.* reported the cracking patterns and shear bands induced by indentation in the representative ZIF-62 glass with the composition $Zn[Im_{1.75}bIm_{0.25}]$, where Im is imidazolate and bIm is benzimidazolate.[14] The shear bands found in the ZIF glass are in strong contrast to the deformation behavior of other types of fully polymerized glasses. Third, To *et al*. measured the fracture toughness of the bulk ZIF-62 glass by using a self-consistent single-edge precracked beam method.[16] The fracture toughness of the glass was found to be ~0.1 MPa $m^{0.5}$, much lower than that of all known brittle oxide and metallic glasses. By combining reactive molecular dynamics simulations and *ab initio* calculations, the unique fracture behavior was attributed to the weak

[a]*Department of Chemistry and Bioscience, Aalborg University, DK-9220 Aalborg, Denmark*
[b]*State Key Laboratory of Silicate Materials for Architectures, Wuhan University of Technology, Wuhan, China*
[c]*Laboratory of Glasses and Ceramics, University of Rennes 1, 35042 Rennes, France*
‡*These authors contributed equally.*
Electronic Supplementary Information (ESI) available: [details of any supplementary information available should be included here]. See DOI: 10.1039/x0xx00000x

Table 1. Comparison of the mechanical properties for the ZIF-62 glasses

Samples	Density (g/cm^3)	Microhardness (GPa)	Nanohardness (GPa)	Reduced modulus (GPa)	Crack resistance (N)	Elastic recovery (%)
Compressed ZIF-62 glass	1.506±0.005	0.59±0.02	0.70±0.03	7.54±0.03	3.8	58.7
Standard ZIF-62 glass	1.481±0.003	0.52±0.02	0.74±0.03	6.77±0.02	3.9	50.4
Annealed ZIF-62 glass	N/A	0.53±0.02	0.67±0.02	6.67±0.02	N/A	50.5

coordinative Zn-N bonds. Despite these findings, the following questions remain unanswered: what is the indentation deformation mechanism of ZIF glass? What structural factors affect indentation deformation?

To answer these questions, we investigated the indentation deformation of ZIF-62 glasses. Nanoindentation was performed to determine the extent of elastic deformation of the glasses. Sub-T_g (where T_g is the glass transition temperature) annealing on indented samples were performed in dry argon gas and subsequently, the indents were imaged using laser scanning microscopy and atomic force microscopy (AFM) to detect the morphology and volume changes of the indents upon annealing. In this way, the ratio of the plastic deformation and densification during indentation can be obtained. By comparing the indentation behaviors of the compressed and the standard ZIF-62 glasses, we studied the effect of structural densification on the crack initiation resistance and hardness of ZIF-62 glasses. Finally, the structural origin of the indentation deformation of ZIF glasses was discussed.

2. Experimental

2.1 Preparation of ZIF-62 glasses

The ZIF-62 crystal was first synthesized by solvothermal method (see Supporting Information). The crystalline nature of the as-prepared ZIF-62 sample was confirmed by X-ray diffraction (XRD), as shown in Fig. S1. The melting temperature (T_m) of ZIF-62 crystal determined by calorimetric measurement is 693 K (Fig. S2).

Subsequently, the ZIF-62 crystal powder was heated to 738 K at 10 K/min and held for 5 min, and then cooled to room temperature in a tube furnace (in inert argon atmosphere) and thereby ZIF-62 glass was obtained (See XRD pattern in Fig. S1 and the glass transition peak in Fig. S2).

This glass was crushed to powder using agate mortar. The powder was used to produce bulk ZIF-62 glass by spark plasma sintering (SPS) under vacuum (HP-D 10 SPS, FCT System GmbH, Germany). Specifically, 0.15 g glass powder was filled into a graphite die (10 mm in diameter) protected by papyex foil and a K-type thermocouple was inserted into a hole in the wall of the die and be touched with the sample. The process chamber was evacuated and the temperature was raised to 593 K at 50 K/min by the resistive heat generated by passing a pulsed direct current (max. 0.35 kA) at 4.65 V through the graphite parts. After the dwelling time of 5 min, the samples were cooled at about 50 $K \cdot min^{-1}$.

Since ZIF-62 glass was subjected to a pressure of 60 MPa during SPS synthesis, we denominated the as-prepared glass as 'compressed glass'. Note that the T_g of the glass obtained at the ambient pressure was measured to be 599 K by a differential scanning calorimeter (DSC). By reheating the compressed glass to 633 K in DSC, and holding it at this temperature for 5 min, we obtained a relaxed glass, which was designated as 'standard glass'. Subsequent to indentation, the standard glass was annealed at $0.9T_g$ in argon for 2 h in order to recover the volume densified by indentation.[17] We refer to this sample as 'annealed ZIF-62 glass'.

2.2 Characterizations

The density of the glasses was measured at room temperature according to the Archimedes' principle with ethanol as the soaking solution. For the indentation measurements, the standard and compressed ZIF-62 glass samples were ground using SiC paper of grit size 2400, and 4000, and finally polished using a suspension of diamond particles with 1 μm. The hardness was measured using Vickers indentation (CB5000, Nanovea) with 0.49 N loading. The loading and unloading rates were set to ascertain 6 sec loading time ($9.8\ N \cdot min^{-1}$), and 15 sec creeps at the highest load was applied. The indent images were subsequently obtained by an optical microscope and the hardness value (H_V) was calculated as:

$$\boldsymbol{H_V = 1.8544 \frac{P}{(\frac{d_1+d_2}{2})^2}}, \quad (1)$$

where P is the load, and d_1 and d_2 are the lengths of the indent diagonals. To evaluate the crack resistance (CR) of the glasses to sharp contact loading, the indentations were performed under various loads (0.1~6 N). Dividing the total number of cracks by the total number of corners (four in each) of the Vickers indents leads to the crack probability at each specific load. Cracking resistance curves were obtained by plotting the crack probability against the load. CR is defined as the load, at which the crack probability is equal to 50%.

To clarify the elastic deformation behavior, we measured the load-displacement curves using nanoindentation experiments. This was done using a Triboindenter instrument (Hysitron, Inc., Minneapolis, MN), which has a high data acquisition rate of up to 104 s^{-1}. The experiments were performed under loads of 1000-4000 μN with a Berkovich tip.

The laser scanning microscopy (Lext OLS 4100, Olympus) was performed on series Vickers indents to observe topographical images

Table 2. Fitting parameters for the loading and unloading curves. The unloading curves were fitted by the power-law proposed by Loubet et al. [Eq. (2)].[25]

Samples	Constant α	Constant *n*	*R*-Square	Young's modulus (GPa)
Compressed ZIF-62 glass	0.88±0.01	1.404±0.002	0.998	6.66±0.03
Standard ZIF-62 glass	0.92±0.01	1.424±0.002	0.999	5.97±0.02

of the indent sites. About 80 different depth of focus images were recorded to generate the 3-dimensional image of an indent. The indentation impressions were also observed using a Ntegra (NT-MDT) AFM. The volume change caused by annealing was measured in tapping mode at room atmosphere (RH ~50%, ~20 °C). The AFM cantilever had a silicon tip with a scanning frequency of 1.4 Hz.

3. Results

Fig. 1a shows the load-displacement (*P*-*h*) curves for the two types of ZIF-62 glasses, i.e., standard and compressed ones. The *P*-*h* curves provide a mechanical fingerprint of the deformation response to indentation load, and mechanical properties such as Young's modulus (*E*) and hardness (*H*) can be obtained.[18-20] Young's modulus can be calculated based on the Oliver-Pharr method.[21] The reduced modulus (E_r) and nano-hardness derived from the nanoindentation measurements, as well as the density and Vicker micro-hardness, are listed in Table I. Compared to the standard ZIF-62 glass, the compressed glass possesses a 2% higher density (Table I), implying that the pressure used during the SPS process densifies the glass structure. Upon reheating to above T_g, the structure of the compressed glass can partially relax. Vickers hardness of the compressed ZIF-62 glass is also higher than that of the standard one, indicating that the pressure-induced densification makes the ZIF-62 glass harder, as found in various oxide glasses.[22,23] However, this enhancement of hardness is not observed in the nanoindentation experiments on the same glasses, likely because the slight difference in hardness values is hidden within the error range of hardness measurements via the nanoindentation due to the indentation size effect. By calculating the displacement difference, i.e., $(h_{max}\text{-}h_f)/h_{max}$, we obtained the elastic deformation of both the compressed and the standard ZIF-62 glasses, which are 58.7% and 50.4%, respectively. This implies that the elastic deformation contributes more than half to the total deformations during indentation.

Next, we consider in more detail the unloading curves that can be used to determine the elastic displacements, contact areas, Young's modulus, and nanohardness. When the unloading curve can be fitted by a power-law relationship [Eq. (2)],[21,24,25] then these mechanical properties can be determined:

$$\boldsymbol{P = \alpha(h - h_f)^n}, \quad (2)$$

where α and *n* are material constants. By using this equation, we fit the unloading curves of the glasses, finding good agreement (*R*-square is 0.99) between the measured and fitted curves (Fig. 1b), implying that the mechanical properties (especially reduced modulus) derived from the nanoindentation measurement are accurate.[21] The fitting parameters are listed in Table II.

Then, based on the Oliver-Pharr method,[21,26,27] the reduced modulus (E_r) of the sample can be derived from unloading data using the following equation:

$$\boldsymbol{E_r = \frac{\sqrt{\pi}}{2}\frac{S}{\beta\sqrt{A}}}, \quad (3)$$

where *S* is the measured stiffness ($S = dP/dh$) of the upper portion of the unloading data, β is the shape constant for the nanoindentation

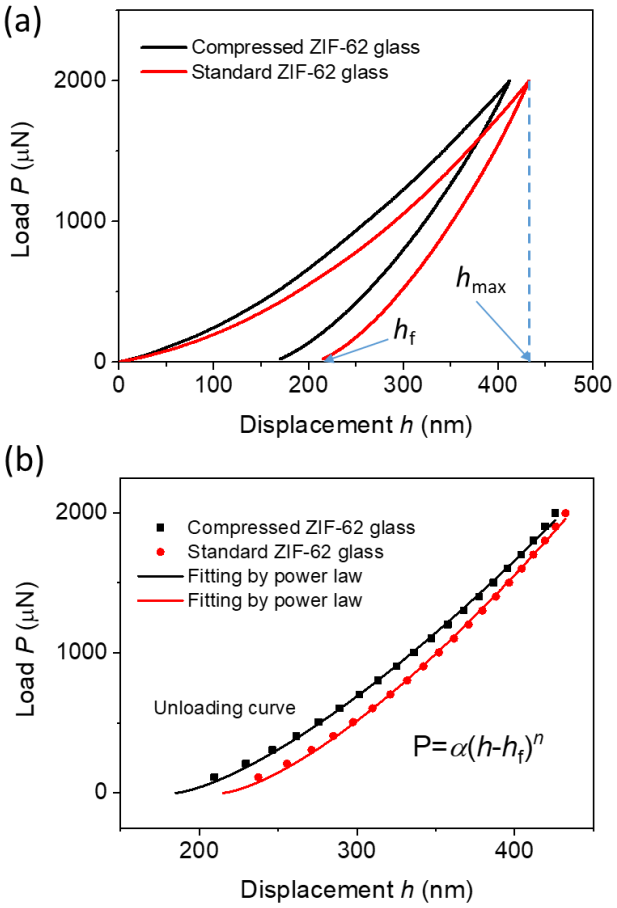

Fig. 1. Load-displacement curves for ZIF-62 glasses. (a) Loading-unloading curves obtained under 2000 μN maximum load for compressed and standard ZIF-62 glass. h_{max} is the maximum displacement at the maximum loading and h_f is the final depth after unloading; (b). Unloading curves for the compressed and standard ZIF-62 glasses. Solid curves: the power-law fits [Eq. (2)].[25]

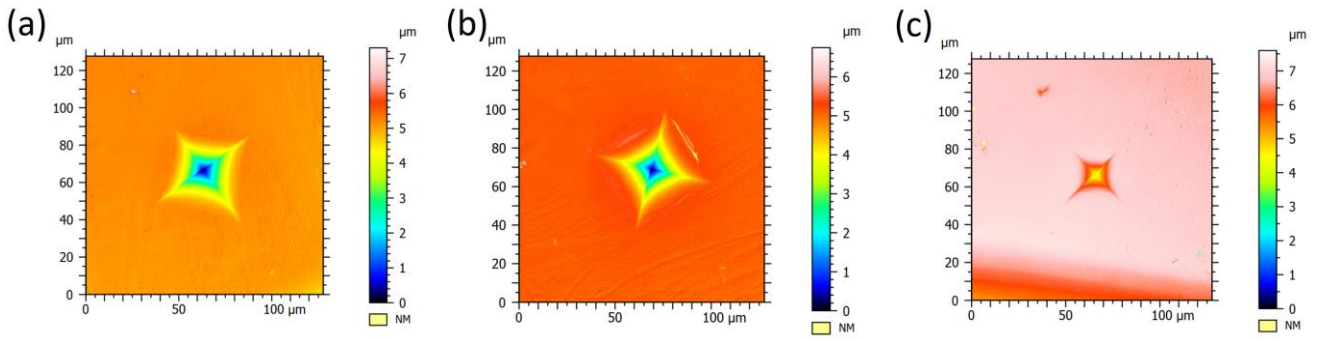

Fig. 2. Laser microscopy images of Vickers indents. (a) Standard, (b) annealed, and (c) compressed ZIF-62 glasses.

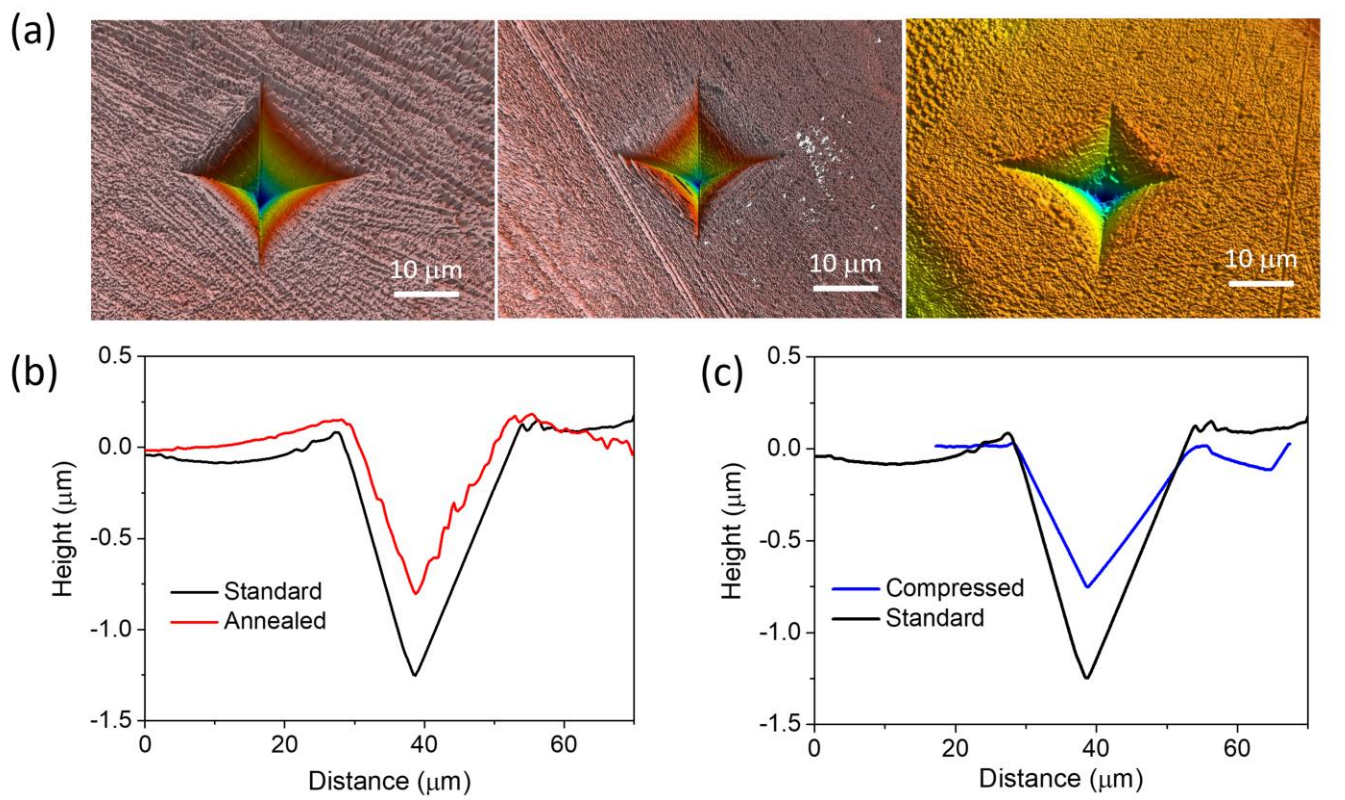

Fig. 3. Three dimensional images and cross-section profiles for indents upon 0.98 N load on the ZIF-62 glasses. (a). 3-D images captured by the laser microscopy for (left to right) the standard, annealed and compressed ZIF-62 glasses; (b). Cross-section profiles obtained by AFM measurements for the standard and annealed ZIF-62 glasses; (c). Cross-section profiles obtained by AFM measurements for the compressed and standard ZIF-62 glasses.

tip (1.034 for the used Berkovich tip), A is the projected area of the elastic contact. Further, Young's modulus (E) of the ZIF-62 glasses could be calculated from the equation[27]:

$$\boldsymbol{E} = \frac{(\mathbf{1}-\nu^2)}{\frac{\mathbf{1}}{E_r}-\frac{1-\nu_i^2}{E_i}}, \quad (4)$$

where ν is Poisson's ratio for the ZIF-62 glasses, E_i and ν_i are the parameters for the diamond indenter, which are 1141 GPa and 0.07, respectively[27]. E_r values have been obtained by using Eq. (3) (See Tab. I). Poisson's ratio of the ZIF-62 glass was reported to be 0.34.[14] Hence, Young's modulus data of ZIF-62 glasses are calculated and listed in Table II.

Fig. 2 shows laser microscopy images of Vickers indents in the three ZIF-62 glasses under the load of 0.98 N. Generally, the shear flow during indentation results in pile-ups around the indent.[4,5] However, from the images of the indents of the ZIF-62 glasses with the depth scale (Fig. 2 and 3a), no clear signs of pile-ups can be observed around the indents. This suggests that a low degree of plastic deformation occurs in ZIF-62 glasses during indentation. The AFM and laser microscopy cross-section profiles (Figs. 3b and c, and Fig. S3) also confirm that there are no pile-ups.

The indent volume of the compressed ZIF-62 is ~40% smaller than that of the standard one (Figs. 3a and 3c), implying that significant pre-densification occurs during the SPS process, which

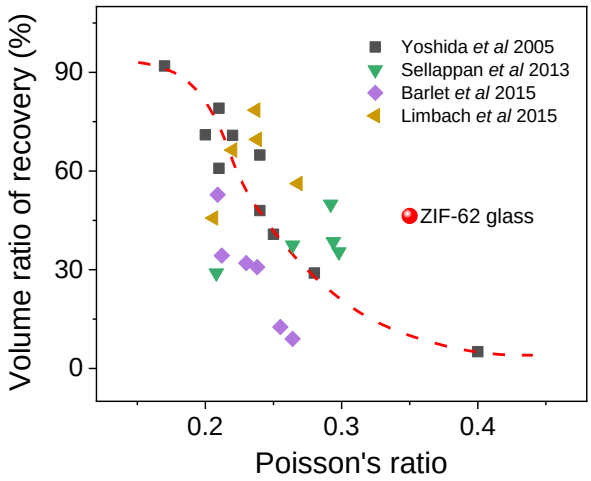

Fig. 4. Relationship between Poisson's ratio and the volume recovery ratio from indentation. Comparison of the data for ZIF-62 glass with that of other reference glasses from refs. 4, 28, 29, 30. Poisson's ratio of ZIF-62 glass is obtained from ref. 14.

could be associated with partial collapse of the framework cavities. This is likely due to the flexibility of the ZIF glass structure with a large size linker and free volume,[9,14] in addition to weak Zn-N coordinative bonds. By performing indentation on the standard glass and subsequently sub-T_g ($0.9T_g$) annealing, we can qualify the densification and plastic shear flow contributions to the total indentation deformation by investigating the volume changes (Fig. 3b).[4,5] In addition, since the densification can induce both reversible and irreversible volume changes, the former can recover upon the sub-T_g annealing. Therefore, by calculating the volume changes upon annealing (Fig. 3b), we can obtain the ratio of densified volume to total deformation volume, and this ratio is so called "volume recovery ratio". The volume recovery ratio of ZIF-62 glass is found to be 48.4 %. Fig. 4 shows the relationship between Poisson's ratio and the volume ratio of recovery for various glasses reported by Satoshi *et al.*.[4] Owning to both high Poisson's ratio (~0.34) of ZIF-62 glass[14] and a volume recovery ratio as high as (most) soda-lime-silicate glasses, the ZIF-62 glass does not obey the general trend of volume recovery ratio vs. Poisson's ratio reported for many glass formers, e.g., silica and metallic glasses. Since the ZIF glass structure differs from that of oxide and metallic glasses, this might explain the deviation, although its exact origin remains unknown. However, we note that such deviation from the general trend has previously been observed in some oxide glasses,[22] indicating that Poisson's ratio is not the only factor affecting the volume recovery ratio. A more quantitative study should be conducted to verify the correlation between the volume recovery ratio and Poisson's ratio as well as the glass structural factors.

Fig. 5 shows the indentation cracking resistance curves for both the compressed and the standard ZIF-62 glasses. As mentioned in the experimental section, *CR* is defined as the load required for generating two radial/median cracks on average, i.e., a 50% crack probability for Vickers indentation.[31] Interestingly, the *CR* values for both compressed and standard samples are almost the same (~3.8 N), as shown in Fig. 5. On the contrary, in most oxide glasses, pre-densification leads to reduced CR due to the pressure-induced decrease in deformation through densification, as the latter in turn is believed to reduce the residual stress that drives indentation cracking.[32]

4. Discussion

We have observed pronounced densification in ZIF-62 glasses during the indentation, with the ratio of densification to the total indentation volume of about 50%. There should be two types of structural changes induced by densification during indentation.[33,34] One involves the breakage of bonds, leading to permanent volume changes, while the other is related to the distortion of structural units and a decrease of the free volume in glass. The latter part of the structural change caused by the densification can recover upon annealing at $0.9T_g$. Compared to the oxide glasses, the easier densification in the ZIF-62 glasses could be ascribed to its three different structural features, i.e., (1) the softer Zn[Im/bIm]$_4$ tetrahedral network constructed by the weaker coordination bonds, (2) larger cavity and (3) the presence of larger ligand.[9,14] This unique structural unit leads to the high flexibility of the structure due to the compressible and rotatable organic units. The pressure could also distorts the medium-range (< 20 Å) structural units involving a group of Zn[ligand]$_4$ tetrahedra. Moreover, the penetration of the sharp indenter could induce the breakage of the weak Zn-N coordinative bonds. Thus, in the area subjected to the load, the glass network is compressed, leading to both the reversible changes (e.g., the rotation of organic ligands and distortion of the tetrahedral network), and the irreversible ones (e.g. the breakage of the local bond induced by high stress). We also note that although the cavities in crystalline ZIF-62 partially collapse during melting, some of these cavities survive and remain in the glass structure, but with smaller sizes (4-8 Å).[35-37] These remaining cavities can be compressed upon indentation, thus contributing to the densification. Furthermore, the existence of numerous cavities also gives rise to a high degree of free

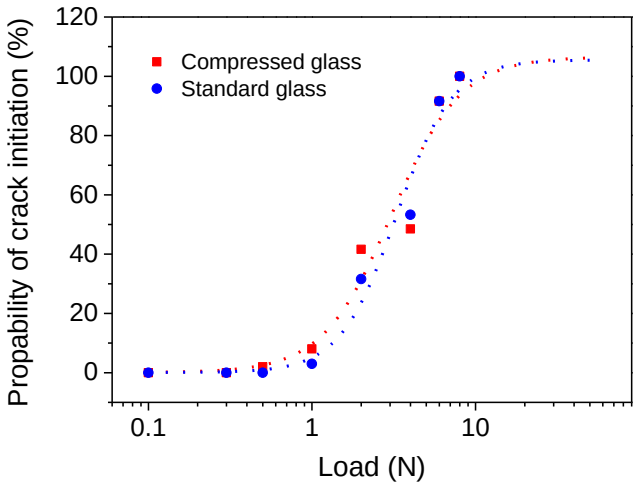

Fig. 5. Crack resistance of the ZIF-62 glasses. Crack probability curves for compressed and standard ZIF-62 glasses.

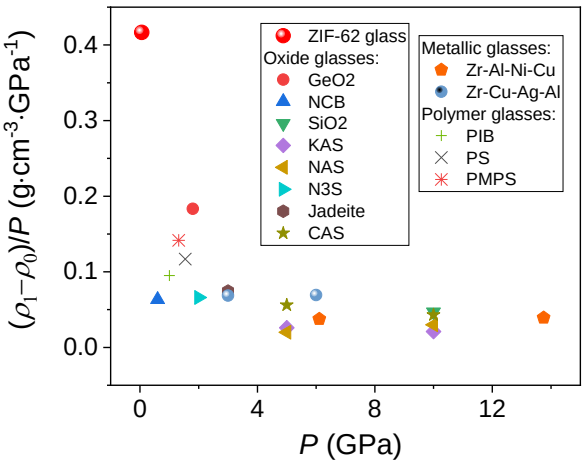

Fig. 6. Pressure dependence of density difference (ρ_1- ρ_0) in glasses. ρ_1 and ρ_0 are the density values of compressed and initial glasses, respectively. ZIF-62 is from this study. Oxide glasses: GeO_2,[38] Na_2O-CaO-B_2O_3 (NCB),[39] Na_2O-B_2O_3-SiO_2 (NBS),[40] SiO_2,[41] CaO-Al_2O_3-SiO_2 (CAS),[42] K_2O-Al_2O_3-SiO_2 (KAS),[42] Na_2O-Al_2O_3-SiO_2 (NAS),[42] Na_2O-$3SiO_2$ (NS3) and Jadeite[43]; Metallic glasses: Zr-Al-Ni-Cu[44] and Zr-Cu-Ag-Al[45]; Polymer glasses: PIB[46], PS[46] and PMPS[46] are taken from publications.

volume in ZIF-62 glass. Although the accurate free volume of ZIF-62 glass cannot be given in this work, we introduce a comparison for the atomic packing density (C_g) for ZIF glass with other kinds of glasses. C_g is the ratio between the volume occupied by the ions and the corresponding effective volume of glass, reflecting the free volume in the glass. The calculation of C_g is provided in the Supporting Information. As shown in Tab. S1, C_g of ZIF-62 glass is found to be 0.08, much lower than that of silica glass (0.45), as well as other glasses. It proves that the free volume of ZIF glass is significantly higher than other glasses. A high degree of free volume in ZIF glass means a low ability to resistant the compression.

The easy densification of the ZIF glass structure is also confirmed by the higher ratio of the density increase ($\Delta\rho$) to the applied pressure (P) for the ZIF-62 glass, compared to oxide glasses (Fig. 6).[38-46] In other words, this is most likely due to the fact that the coordination bonds in the former are much weaker than the ionic-covalent bonds in the latter.[14]

The high flexibility of Zn[ligand]$_4$ tetrahedra[47] gives rise to glass structure with a high degree of elastic deformation, i.e., the ZIF glass network undergoes a certain extent of distortion at the early stage of the loading. Moreover, large organic ligands can also be subjected to a certain degree of distortion, leading to a change in their morphology upon pressure. In other words, the high flexibility of the ZIF glass structure contributes to the elastic deformation during indentation. Hence, we observe the pronounced elastic deformation for ZIF-62 glass during indentation.

Upon indentation, the plastic deformation can induce an upwards slippage in oxide and metallic glasses, leading to pile-ups around the indents.[48-50] However, almost no pile-ups are observed in ZIF-62 glasses upon indentation, implying that the shear flow gives little contribution to the indentation deformation. This behavior is evidently similar to that in silica glass.[51] The extent of pile-up during indentation is affected by multiple structural factors. Specially, for the studied ZIF glass, three structural factors should be related to the lack of pile-ups. (1) The remaining cavities with size of 4-8 Å in the ZIF glass structure after melt-quenching,[35-37] and the remarkably low C_g value indicate that ZIF glass has higher free volume compared to other glasses. It is well known that glasses with high free volume possess a lower tendency to pile-up.[51] (2) It has been reported that glasses with high propensity to densify during indentation do not show pile-ups,[52] since such glass structure exhibits densification rather than shear flow. The ZIF glass network can be easily densified due to the weak Zn-N coordination bonds (compared to the ionic-covalent bonds in oxide glasses), which fracture easily upon mechanical loading.[16] Moreover, the high free volume also contributes to the easy densification, leading to the significant local deformation rather shear flow. (3) It has been suggested that the indentation induced shear flow in glass is correlated with the viscous behavior of the corresponding melt.[53] Specifically, for a glass that undergoes no shear flow during indentation, its liquid state often possesses relatively high viscosity that hinders the translational motion of the involved structural units. Silica glass and ZIF-62 glass both possess very high viscosity at T_m ($10^{5.5}$ and 10^5 Pa·s, respectively).[54]

According to previous studies,[28,55] densification dominates the indentation deformation of oxide glasses with low Poisson's ratio (< 0.25) or relatively high network polymerization degree, i.e., those with low modified contents, whereas the shear flow is more predominant for glasses with high Poisson's ratio. However, ZIF-62 glass exhibits a pronounced densification and only a minor extent of shear flow upon indentation, although it possesses a relative high Poisson's ratio (~0.34) and a fully polymerized network. This anomalous phenomenon could be attributed to the following scenarios. In contrast to the tetrahedral [SiO_4] unit in oxide glasses, the tetrahedral structural unit in ZIF glasses is much bigger, because they are constituted by a metallic node (Zn) and four Im/bIm ligands that are significantly bigger than oxygen. Thus, the structure of ZIF-62 glass is easier to be distorted and densified under mechanical load, rather than shear deformation despite its higher Poisson's ratio (0.34) compared to the polymerized oxide glasses. Moreover, the weaker Zn-N bonds are also the reason for the high degree of densification and only limited shear flow since such bonds readily break and thereby easily induce a deformation of medium-range structure.[9]

5. Conclusions

Based on the indentation study of ZIF-62 glass, we found that more than 50% of the total deformation during load-unloading arises from the elastic deformation, while the densification dominates the permanent volume change during indentation. The easier densification of ZIF-62 glass (compared with other types of network glasses such as silicate glasses) is attributed to both the higher flexibility of the glass network and the higher porosity. Interestingly, the shear flow does not occur in ZIF-62 during indentation, and this distinct feature can be ascribed to three structural factors: high free volume, easily densified

structure and strong steric hindrance of the fully polymerized network structure. The lack of shear flow during indentation is indirectly connected with the significantly higher viscosity of ZIF-62 glass compared with other not-fully polymerized network glasses.

Conflicts of interest

There are no conflicts to declare.

Acknowledgements

This work was supported by VILLUM Fonden (grant no. 13253) and National Natural Science Foundation of China (No. 51802236).

References

1 J. Sehgal and S. Ito, Brittleness of glass, *J. Non-Cryst. Solids*, 1999, **253**, 126-132.

2 T. Rouxel and S. Yoshida, The fracture toughness of inorganic glasses, *J. Am. Ceram. Soc.* 2017, **100**, 4374 -4396.

3 S. Yoshida, Indentation deformation and cracking in oxide glass –toward understanding of crack nucleation, *J. Non-Cryst. Solids X*, 2019, **1**, 100009.

4 S. Yoshida, J.-C. Sanglebœuf and T. Rouxel, Quantitative evaluation of indentation-induced densification in glass, *J. Mater. Res.*, 2005, **20**, 3404 -3412.

5 C. Hermansen, J. Matsuoka, S. Yoshida, H. Yamazaki, Y. Kato and Y. Z. Yue, Densification and plastic deformation under microindentation in silicate glasses and the relation to hardness and crack resistance, *J. Non-Cryst. Solids*, 2013, **364**, 40-43.

6 G. A. Rosales-Sosa, A. Masuno, Y. Higo and H. Inoue, Crack-resistant Al_2O_3–SiO_2 glasses, *Sci. Rep.*, 2016, **6**, 23620.

7 T. M. Gross and M. Tomozawa, "Crack-free high load Vickers indentation of silica glass," *J. Non-Cryst. Solids*, 2008, **354**, 5567-5569.

8 V. Le Houérou, J. C. Sangleboeuf, S. Dériano, T. Rouxel and G. Duisit, Surface damage of soda–lime–silica glasses: indentation scratch behavior, *J. Non-Cryst. Solids*, 2003, **316**, 54-63.

9 T.D. Bennett, J.-C. Tan, Y. Z. Yue, E. Baxter, C. Ducati, N. J. Terrill, H. H. -M. Yeung, Z. Zhou, W. Chen and S. Henke, Hybrid glasses from strong and fragile metal-organic framework liquids, *Nat. Commun.*, 2015, **6**, 8079.

10 H. Hayashi, A. P. Cote, H. Furukawa, M. O'Keeffe and O. M. Yaghi, Zeolite A imidazolate frameworks, *Nat. Mater.*, 2007, **6**, 501-506.

11 K. S. Park, Z. Ni, A. P. Côté, J. Y. Choi, R. Huang, F. J. Uribe-Romo, H. K. Chae, M. O'Keeffe and O. M. Yaghi, Exceptional chemical and thermal stability of zeolitic imidazolate frameworks, *Proc. Natl. Acad. Sci. U.S.A.*, 2006, **103**, 10186-10191.

12 R. S. K. Madsen, A. Qiao, J. Sen, I. Hung, K. Chen, Z. Gan, S. Sen and Y. Z. Yue, Ultrahigh-field ^{67}Zn NMR reveals short-range disorder in zeolitic imidazolate framework glasses, *Science*, 2020, **367**, 1473-1476.

13 G. N. Greaves, S. Sen, Inorganic glasses, glass-forming liquids and amorphizing solids, *Adv. Phys.*, 2007, **56**, 1-166.

14 M. Stepniewska, K. Januchta, C. Zhou, A. Qiao, M. M. Smedskjaer and Y. Z. Yue, Observation of indentation-induced shear bands in a metal–organic framework glass, *Proc. Natl. Acad. Sci. U.S.A.*, 2020, **117**, 10149-10154.

15 S. Li, R. Limbach, L. Longley, A. A. Shirzadi, J. C. Walmsley, D. N. Johnstone, P. A. Midgley, L. Wondraczek and T. D. Bennett, Mechanical properties and processing techniques of bulk metal-organic framework glasses, *J. Am. Chem. Soc.*, 2019, **141**, 1027-1034.

16 T. To, S. S. Sørensen, M. Stepniewska, A. Qiao, L. R. Jensen, M. Bauchy, Y. Z. Yue and M. M. Smedskjaer, Fracture toughness of a metal-organic framework glass, *Nat. Commun.*, 2020, **11**, 2593.

17 S. Yoshida, J.-C. Sanglebœuf and T. Rouxel, Indentation-induced densification of soda-lime silicate glass, *Int. J, Mater. Res.*, 2007, **98**, 360-364.

18 M. R. VanLandingham, J. S. Villarrubia, W. F. Guthrie and G. F. Meyers, Nanoindentation of polymers: an overview, *Macromol. Symp.*, 2001, **167**, 15-44.

19 B. Bhushan and V. N. Koinkar, Nanoindentation hardness measurements using atomic force microscopy, *Appl. Phys. Lett.*, 1994, **64**, 1653-1655.

20 S. V. Hainsworth, H. W. Chandler and T. F. Page, Analysis of nanoindentation load-displacement loading curves, *J. Mater. Res.*, 2011, **11**, 1987-1995.

21 W. C. Oliver and G. M. Pharr, An improved technique for determining hardness and elastic modulus using load and displacement sensing indentation experiments, *J. Mater. Res.*, 1992, **7**, 1564-1583.

22 S. Kapoor, L. Wondraczek and M. M. Smedskjaer, Pressure-induced densification of oxide glasses at the glass transition, *Front. Mater.*, 2017 **4**, 1.

23 Z. Zhang, N. Soga and K. Hirao, Indentation deformation and fracture of densified silicate glass, *J. Mater. Sci.*, 1995, **30**, 6359-6362.

24 M. F. Doerner and W. D. Nix, A method for interpreting the data from depth-sensing indentation instruments, *J. Mater. Res.*, 2011, **1**, 601-609.

25 J. L. Loubet, J. M. Georges, and J. Meille, in Microindentation Techniques in Materials Science and Engineering, edited by P. J. Blau and B. R. Lawn (American Society for Testing and Materials, Philadelphia, 1986).

26 A. C. Fischer-Cripps, Nanoindentation. (Springer, Verlag New York, 2011), p.282.

27 T. H. Wang, T-. H. Fang, and Y. C. Lin, A numerical study of factors affecting the characterization of nanoindentation on silicon Mater. *Sci. Eng. A*, 2007, **447**, 244.

28 P. Sellappan, T. Rouxel, F. Celarie, E. Becker, P. Houizot and R. Conradt, Composition dependence of indentation deformation and indentation cracking in glass, *Acta Mater.*,2013, **61**, 5949-5965.

29 M. Barlet, J.-M. Delaye, T. Charpentier, M. Gennisson, D. Bonamy, T. Rouxel and C. L. Rountree, Hardness and toughness of sodium borosilicate glasses via Vickers's indentations, *J. Non-Cryst. Solids*, 2015, **417**, 66-79.

30 R. Limbach, A. Winterstein-Beckmann, J. Dellith, D. Möncke and L. Wondraczek, Plasticity, crack initiation and defect resistance in alkali-borosilicate glasses: From normal to anomalous behavior, *J. Non-Cryst. Solids*, 2015, **417**, 15-27.

31 T. To, L. R. Jensen and M. M. Smedskjaer, On the relation between fracture toughness and crack resistance in oxide glasses, *J. Non-Cryst. Solids*, 2020, **534**, 119946.

32 T. Rouxel, Driving force for indentation cracking in glass: composition, pressure and temperature dependence, *Philos. T. R. Soc. A*, 2015, **373**, 20140140.

33 A. Arora, D. B. Marshall, B. R. Lawn and M. V. Swain, Indentation deformation/fracture of normal and anomalous glasses, *J. Non-Cryst. Solids*, 1979, **31**, 415-428.

34 U. Ramamurty, S. Jana, Y. Kawamura and K. Chattopadhyay, Hardness and plastic deformation in a bulk metallic glass, *Acta Mater.*, 2005, **53**, 705-717.

35 C. Zhou, L. Longley, A. Krajnc, G. J. Smales, A. Qiao, I. Erucar, C. M. Doherty, A. W. Thornton, A. J. Hill, C. W. Ashling, O. T. Qazvini, S. J. Lee, P. A. Chater, N. J. Terrill, A. J. Smith, Y. Z. Yue, G. Mali, D. A. Keen, S. G. Telfer and T. D. Bennett, Metal-organic framework glasses with permanent accessible porosity, *Nat. Commun.*, 2018, **9**, 5042.

36 L. Frentzel-Beyme, M. Kloß, R. Pallach, S. Salamon, H. Moldenhauer, J. Landers, H. Wende, J. Debus and S. Henke, Porous purple glass- a cobalt imidazolate glass with accessible porosity from a meltable cobalt imidazolate framework, *J. Mater. Chem. A*, 2019, **7**, 985-990.

37 A. W. Thornton, K. E. Jelfs, K. Konstas, C. Doherty, A. Hill, A. Cheetham and T. D. Bennett, Porosity in metal-organic framework glasses, *Chem. Commun.*, 2016, **52**, 3750-3753.

38 S. K. Sharma, D. Virgo and I. Kushiro, Relationship between density, viscosity and structure of GeO_2 melts at low and high pressures, *J. Non-Cryst. Solids*, 1979, **33**, 235-248.

39 M. M. Smedskjaer, R. E. Youngman, S. Striepe, M. Potuzak, U. Bauer, J. Deubener, H. Behrens, J. C. Mauro and Y. Z. Yue, Irreversibility of pressure induced boron speciation change in glass, *Sci. Rep.*, 2014, **4**, 3770.

40 L. Wondraczek, S. Sen, H. Behrens, R. E. Youngman, Structure-energy map of alkali borosilicate glasses: Effects of pressure and temperature, *Phy. Rev. B*, 2007, **76**, 014202.

41 D. Wakabayashi, N. Funamori, T. Sato and T. Taniguchi, Compression behavior of densified SiO_2 glass, *Phy. Rev. B*, 2011, **84**, 144103.

42 J. R. Allwardt, J. F. Stebbins, B. C. Schmidt, D. J. Frost, A. C. Withers and M. M. Hirschmann, Aluminum coordination and the densification of high-pressure aluminosilicate glasses, *Am. Mineral.*, 2005, **90**, 1218-1222.

43 S. Bista, J. F. Stebbins, W. B. Hankins and T. W. Sisson, Aluminosilicate melts and glasses at 1 to 3 GPa: Temperature and pressure effects on recovered structural and density changes, *Am. Mineral.*, 2015, **100**, 2298-2307.

44 T. Mashimo, H. Togo, Y. Zhang, Y. Uemura, T. Kinoshita, M. Kodama and Y. Kawamura, Hugoniot-compression curve of Zr-based bulk metallic glass, *Appl. Phys. Lett.*, 2006, **89**, 241904.

45 W. Liu, Q. Zeng, Q. Jiang, L. Wang and B. Li, Density and elasticity of $Zr_{46}Cu_{37.6}Ag_{8.4}Al_8$ bulk metallic glass at high pressure, *Scripta Mater.*, 2011, **65**, 497-500.

46 L. Hong, B. Begen, A. Kisliuk, C. Alba-Simionesco, V. N. Novikov and A. P. Sokolov, Pressure and density dependence of the boson peak in polymers, *Phys. Rev. B*, 2008, **78**, 134201.

47 M. T. Wharmby, S. Henke, T. D. Bennett, S. R. Bajpe, I. Schwedler, S. P. Thompson, F. Gozzo, P. Simoncic, C. Mellot-Draznieks, H. Z. Tao, Y. Z. Yue and A. K. Cheetham, Extreme flexibility in a zeolitic imidazolate framework: porous to dense phase transition in desolvated ZIF-4, *Angew. Chem. Int. Ed.*, 2015, **54**, 6447-6551.

48 R. Bhowmick, R. Raghavan, K. Chattopadhyay and U. Ramamurty, Plastic flow softening in a bulk metallic glass, *Acta Mater.*, 2006, **54**, 4221-4228.

49 B. Taljat and G. M. Pharr, Development of pile-up during spherical indentation of elastic-plastic solids, *Int. J. Solids Struct.*, 2004, **41**, 3891-3904.

50 G. Das, S. Ghosh, S. Ghosh and R. N. Ghosh, Materials characterization and classification on the basis of materials pile-up surrounding the indentation, *Mater. Sci. Eng. A*, 2005, **408**, 158-164.

51 J. A. Howell, J. R. Hellmann, C. L. Muhlstein, Correlations between free volume and pile-up behavior in nanoindentation reference glasses, *Mate. Lett.*, 2008, **62**, 2140-2142.

52 C. R. Kurkjian, G. W. Kammlott, and M. M. Chaudhri, Indentation behavior of soda-lime silica glass, fused silica, and single-crystal quartz at liquid nitrogen temperature, *J. Am. Ceram. Soc.,* 2015, **78**, 737.

53 J. Kjeldsen, M. M. Smedskjaer, M. Potuzak and Y. Z. Yue, Role of elastic deformation in determining the mixed alkaline earth effect of hardness in silicate glasses, *J. Appl. Phys.*, 2015, **117**, 034903.

54 A. Qiao, T. D. Bennett, H. Tao, A. Krajnc, G. Mali, C. M. Doherty, A. W. Thornton, J. C. Mauro, G. N. Greaves and Y. Z. Yue, A metal-organic framework with ultrahigh glass-forming ability, *Sci. Adv.*,2018, **4**, eaao6827.

55 T. Rouxel, H. Ji, J.P. Guin, F. Augereau and B. Rufflé, Indentation deformation mechanism in glass: Densification versus shear flow, *J. Appl. Phys.*, 2010, **107**, 094903.